Available online at www.sciencedirect.com
SCIENCE DIRECT
Solid State Communications 137 (2006) 49–52
solid state communications
www.elsevier.com/locate/ssc

Critical point transitions of wurtzite indium nitride

W.Z. Shen [a,*], X.D. Pu [a], J. Chen [a], H. Ogawa [b], Q.X. Guo [b]

[a] *Laboratory of Condensed Matter Spectroscopy and Opto-Electronic Physics, Department of Physics, Shanghai Jiao Tong University, 1954 Hua Shan Road, Shanghai 200030, People's Republic of China*

[b] *Department of Electrical and Electronic Engineering, Faculty of Science, and Engineering, Saga University, Saga 840-8502, Japan*

Received 2 June 2005; accepted 24 October 2005 by S. Das Sarma

Abstract

The optical transmission, photoluminescence, and reflection spectra have been measured on a high-quality wurtzite indium nitride (InN) single crystal in the range of 0.5–20.0 eV. The fundamental bandgap of intrinsic InN has been extracted by taking into account the Burstein–Moss shift, bandgap renormalization and Urbach band tail effects, and found to be very close to the recent strongly re-established value of ~1.2 eV. With the aid of Adachi's dielectric function model for the vacuum ultraviolet reflection spectra and the empirical pseudopotential method approach for the electron band-structure, we are able to identify up to nine electronic transitions, showing clear picture for the critical point transitions in InN. The temperature dependence of these interband transitions has also been revealed.

PACS: 78.40Fy; 71.20Nr; 78.55.Cr; 78.66Hf

Keywords: D. Critical point transitions; A. Indium nitride; A. Wurtzite

Recently, indium nitride (InN) has received intensive research interest mainly due to its possible applications in high-speed/high-frequency electronics and solar cells. However, the growth of high-quality InN remains a formidable challenge due to the low-dissociation temperature of InN and the extremely high-equilibrium vapor pressure of nitrogen. As a result, many of its fundamental parameters are still not well known despite the detailed investigation since the 1980s. The study of critical points (CPs) in InN will give a clear understanding of optical transition processes and electron band-structures, which is not only of scientific interest, but also important for device applications.

The long-time established bandgap was ~1.9 eV for polycrystalline InN films grown by sputtering [1]. The recent infrared photoluminescence (PL) and optical absorption on single crystal InN grown by molecular-beam epitaxy (MBE) [2,3] and metal-organic vapor phase epitaxy (MOVPE) [4] revealed the bandgap energy of ~0.7 eV, which was considered as unambiguous evidence for the narrow gap nature of InN. Nevertheless, this kind of assignment seems to be rather simplistic, since the origin of the dramatic bandgap deviation is most likely related to the precipitation of indium in the metallic phase that leads to additional optical losses associated with the Mie resonances in the metallic clusters [5]. Actually, the possibility of a ~1.2 eV bandgap has been strongly re-established for InN [6], and the very recent resonant Raman measurements on these MBE InN clearly indicates the presence of an InN critial point within ~0.2–0.3 eV below 1.5 eV [7]. We have also demonstrated that it is not accurate in the assignment of ~0.7 eV fundamental bandgap for intrinsic InN simply from PL and absorption data, since strong room-temperature PL at 1.87 eV, together with a clear absorption edge at 1.97 eV, has been observed in InN grown by reactive sputtering [8].

In comparison with the extensive experimental studies of the critical point E_0, there are few references in the literature up to now concerned with the high order CPs in InN. Kasic et al. [9] have employed the spectroscopic ellipsometry to study the InN dielectric function up to 6.5 eV at room temperature. In combination with the theoretical band-structures, they have summarized the CPs of InN along with literature data at ~4.8, 5.4, 5.6, and 6.1 eV, as well as the fundamental bandgap. We have reported the reflection spectra of InN single crystals in the photon energy from 2 to 130 eV with synchrotron radiation for the optical constants using Kramers–Kronig analysis [10].

* Corresponding author. Tel.: +86 21 54743242; fax: +86 21 54741040.
E-mail address: wzshen@sjtu.edu.cn (W.Z. Shen).

0038-1098/$ - see front matter © 2005 Elsevier Ltd. All rights reserved.
doi:10.1016/j.ssc.2005.10.016

Furthermore, band-structure of InN has also been widely studied by a number of theoretical models over the past 20 years, such as the ab initio calculations [11], and empirical pseudopotential method (EPM) approach [12–14], to follow the experimental investigation, especially at the recent fundamental bandgap debate. The re-establishment of the ~1.2 eV InN bandgap has called for a re-examination of the InN band-structures. The aim of this communication is to report reliable experimental optical transitions in single crystal wurtzite InN thin films in the spectral range of 0.5–20.0 eV, on the basis of successful extraction the bandgap of ~1.2 eV from the optical transmission and PL measurements. With the aid of Adachi's dielectric function model [15] for the reflection spectra and the EPM approach [14] for the band-structure, we are able to identify up to nine electronic transitions, and therefore present clear picture for the CPs in InN.

The studied InN thin films were grown on (0001) α-Al_2O_3 substrates by microwave-excited MOVPE at growth temperature of 500 °C [16]. Reflection high-energy electron diffraction results showed all the InN samples to be a single crystalline and to have an orientation relationship of (0001) InN||(0001) α-Al_2O_3. Only two diffraction peaks corresponding to the (0002) and (0004) reflections from InN were observed in the θ–2θ profiles, indicating that the c-axis of InN is perpendicular to the substrate surface. The unintentionally doped InN films (thickness of 0.35 μm) exhibits n-type conductivity, with Hall mobility of 365 $cm^2/V\,s$ and electron concentration (n) of $2.8\times10^{19}\ cm^{-3}$ at room temperature. Temperature-dependent transmission/reflection measurements were carried out on a Nicolet Nexus 870 Fourier transform infrared (FTIR) spectrometer (Si detector for infrared region) and Jobin Yvon 460 monochromator (Hamamatsu photomultiplier tube for visible and ultraviolet regions), while the PL spectra were taken with an Ar^+ laser (514.5 nm) under a Jobin Yvon LabRAM HR 800 VIS-NIR micro-Raman system with an Andor DU420 classic CCD detector for visible region and the Nexus 870 FTIR with an InGaAs detector for infrared region. Vacuum ultraviolet (VUV) reflection spectra were measured between 4 and 20 eV at the beam line of the SOR-RING in the Institute for Solid State Physics of the University of Tokyo with a 1-m Seya-Namioka type monochromator [17].

Fig. 1 shows the experimental temperature-dependent (a) optical transmission (solid squares) and (b) PL spectra of the InN thin film. By the aid of a detailed calculation of the transmission profiles taking into account both the intrinsic square-root absorption and the Urbach exponential absorption edge [18], we are able to demonstrate a fairly good agreement between the calculated solid curves and experimental data in Fig. 1(a). Through the calculation, we can obtain a lot of optical information about the InN thin film, such as temperature-dependent transmission bandgap $E_{gTR}(T) = 1.502\text{–}2.93\times10^{-4}\,T^2/(T+580)$ (eV), temperature- and wavelength-dependent refractive index (2.83–2.72 from 10 to 300 K at E_{gTR}) and absorption coefficient ($5\text{–}7\times10^4\ cm^{-1}$ from 10 to 300 K at E_{gTR}), as well as Urbach band tail parameter $E_U = 84.8 + 0.00454T^{3/2} + 3.90\coth(425/T)$ (meV). The yielded E_{gTR} at different temperatures has also been marked in Fig. 1(a) by arrows.

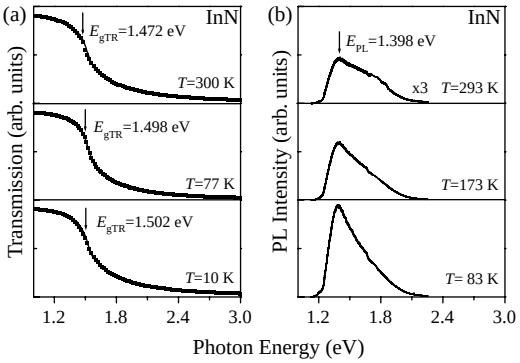

Fig. 1. Temperature-dependent (a) optical transmission and (b) PL spectra of the wurtzite InN thin film grown by MOVPE on sapphire (0001) substrate. For transmission spectra, experimental data: solid squares, calculated results: solid curves.

We note that the InN sample exhibits intense room-temperature luminescence [Fig. 1(b)] with peak energy E_{PL} close to E_{gTR}. No luminescence signal can be detected around 0.7 eV. We have also observed the same temperature- and excitation power-dependences of the PL characteristics as reported previously for MBE InN [3,19,20]. The peak energy does not show any significant shift with the increase of temperature due to the PL lineshape broadening and weak temperature dependence of the InN bandgap (only ~30 meV from 10 to 300 K). The integrated PL intensity depends linearly on the excitation power over three orders of magnitude. The PL peak energy exhibits a slight blueshift with the increase of excitation power due to the bandfilling effects. Emission spectra with such behaviors have been typically observed in highly doped semiconductors and they are characteristic for radiative recombination between the degenerate electrons in the conduction band and the nonequilibrium holes located in the valence band tails. The change of the lineshape in the high-energy side reflects the thermal excitation of electrons near the Fermi level and additional thermal broadening effect.

It should be noted that, due to the high-electron concentration, the present InN thin films (including the reported ones in the literature) are normally in a degenerate condition. The optical absorption occurs between the states in the valence band and the states above the Fermi level in the conduction band under the momentum (**k**) selection rule, while the luminescence represents the recombination of electrons distributed up to the Fermi level with the localized holes in the tail states without conserving **k**. Therefore, the above observed E_{gTR} and E_{PL} do not reflect the true bandgap (E_g) of intrinsic InN. Nevertheless, E_g can be deduced from E_{gTR} and E_{PL} after a careful consideration of the Burstein–Moss shift (through the electron effective mass from Kane's two band $\mathbf{k}\cdot\mathbf{p}$ model with conduction band nonparabolicity [21] and hole effective mass of 0.30 m_0 [19]), bandgap renormalization effect (by $1.7\times10^{-8}n^{1/3}$ eV [22]), as well as the Urbach band tail effect (from the above transmission E_U results for PL peak only). At room temperature, the yielded

E_g is 1.213 eV from E_{gTR} and 1.223 eV from E_{PL}. We notice that there is only 10 meV difference for the deduced bandgap of intrinsic InN between the optical transmission and PL measurements, and the value of $\sim$1.2 eV is also in good agreement with the recent strongly recommended parameter for InN [6], as well as the resonant Raman results [7]. This also indicates that, in our MOVPE sample, the effect of indium rich regions implicated in the $\sim$0.7 eV absorption and emission features [5,6] of MBE InN is trivial. Based on the above argument, we can further modify the temperature-dependent intrinsic InN bandgap from the transmission data as: $E_g(T) = 1.243 - 2.93 \times 10^{-4} T^2/(T + 580)$ (eV).

Fig. 2(a) displays the room-temperature VUV reflection spectrum of the wurtzite InN thin film with the photon energy from 4 to 20 eV. The solid squares are the experimental data, while the solid curve is the calculated spectrum employing Adachi's dielectric function model [15], showing a fairly good agreement with the experimental data. In the calculation of reflection spectrum, the normal incident reflectivity is calculated after obtaining the complex dielectric function $\varepsilon(\hbar\omega) = \varepsilon_1(\hbar\omega) + i\varepsilon_2(\hbar\omega)$, which can be described by the sum of terms corresponding to the following contributions: (i) the lowest-direct gap E_0 CP transition ε_0 and the excitonic transition ε_{0x} at E_0 CP; (ii) E_1 CP transition ε_1 and the excitonic transition ε_{1x} at E_1 CP; (iii) higher lying CP transitions ε_h, and (iv) the additive constant $\varepsilon_1(\infty)$, which arises from the transitions beyond the spectral range.

Fig. 2(b) shows the calculated imaginary of the complex dielectric function ε_2. The shape of the ε_2 spectrum is quite similar to that of the reflection spectrum in Fig. 2(a). However, the former reflects clearer image of the transitions at the CPs than that of the latter. For better analysis, each contribution to ε_2 has been plotted separately by the dotted curves and marked by the arrows. We can observe seven clear transition structures (marked from A to G) in the experimental VUV reflection spectrum. Though a number of calculations have been performed on the electron band-structure of InN, the EPM approach by Fritsch et al. [14] yields a complete and reliable band dispersion of valence and conduction bands, and the CPs in EPM band-structure can describe quite well all the major structures in our reflection spectra. The theoretical band-structure of AlN by the same research group has also been explained well our experimental CPs in wurtzite AlN [23].

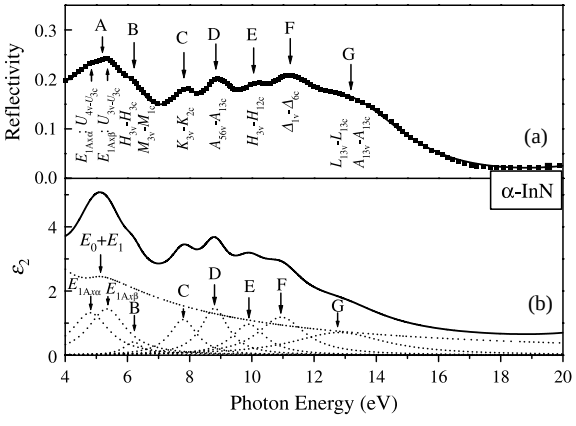

Fig. 2. (a) Reflection spectrum with photon energy from 4 to 20 eV of a wurtzite InN single crystal at room temperature. Experimental data: solid squares, the fitted results using Adachi's dielectric function model: solid curve. (b) The calculated imaginary of dielectric function ε_2 of InN (solid curve). The contribution of all the observed CP transitions to ε_2 has been shown as the dotted curves.

The above discussed InN direct bandgap of E_0 transition in the optical transmission and PL spectra occurs in the center of the Brillion zone (Γ point), which will be $\sim$1.24 eV in intrinsic InN at very low temperature. We note that the uppermost valence band at Γ point of wurtzite InN is the single-degenerate state (Γ_6), lifted by the spin–orbit splitting and the hexagonal symmetry crystal-field splitting, so the direct bandgap of E_0 corresponds to the transition of $\Gamma_{6v} - \Gamma_{1c}$ in the InN band-structure. Considering the lowest direct bandgap of 0.79 eV in the EPM band-structure [14], we have to self-correct a 'scissors operator' (constant shift) of 0.45 eV in the band-structure, in order to have more precise analysis later along.

The structure A labeled in our reflection spectra can be assigned correspondingly to the E_1 CP transition compared with the EPM band-structure [14], which usually occurs at the saddle point inside the zone of the (111) direction (U point). Through calculation, two fitting peaks with the photon energies around 4.90 and 5.43 eV at room temperature are involved in the broad structure A. The contributions of these two peaks to the structure A can be clearly seen from the dielectric function spectrum in Fig. 2(b). The two structures (labeled by $E_{1A\times\alpha}$ and $E_{1A\times\beta}$ in Fig. 2) can be well assigned to the transitions of $U_{4v} - U_{3c}$ and $U_{3v} - U_{3c}$, respectively. Furthermore, our temperature-dependent reflection measurements reveal that the transition energy of $E_{1A\times\beta}$ blueshifts with decreasing temperature, while the transition energy of $E_{1A\times\alpha}$ is almost unchanged, originating from the different electronic configuration states at U_{4v} and U_{3v}.

From the viewpoint of dielectric function models, high-lying transitions are characterized with a certain number of damped harmonic oscillators [Fig. 2(b)] and the calculated oscillator energies represent the center positions of the structures in the reflection curve. Structure B in the spectrum appears to be a shoulder around 6.2 eV. More than one CP transition are possibly involved within that energy region, since, in principle, all of the allowed CP transitions from the valence band to the conduction band can take place simultaneously and be recorded in the reflection spectra. It is reasonable to ascribe such structures to be the contributions from several energy-gap-closed transitions, instead of one single transition. Here, we list two main CP transitions $H_{3v} - H_{3c}$ (6.19 eV) and/or $M_{3v} - M_{1c}$ (6.27 eV), which may contribute to the structure B. It should be noted that Kasic et al. [9], by the aid of the same EPM band-structure, have also identified these CP features around 4.8, 5.4, 5.6, and 6.1 eV in their spectroscopic ellipsometry spectra, and summarized all the previously reported CP results of InN.

We now focus on the higher energy region from 7.0 to 20.0 eV in the VUV reflection spectrum, where several higher lying structures are clearly observed. These structures are labeled from C to G [Fig. 2], which have never been concerned

in the literature so far. In Fig. 2(a), we mark these reflection structures and their relation to the main CP transitions in the EPM band-structure [14], by comparing our experimental data with the calculated results for each of the main CP transitions. From the photon energy point of view, each reflection peak from C to F can be clearly identified with one transition. The calculated structure positions at room temperature are 7.80, 8.80, 9.90, and 10.95 eV for peak C to F, respectively. As the higher lying energy positions are insensitive to the temperature in III-nitrides [23], compared with the EPM band-structure, they can be attributed to the transitions of $K_{3v}-K_{2c}$ (7.98 eV), $A_{56v}-A_{13c}$ (8.87 eV), $H_{3v}-H_{12c}$ (9.84 eV), and $\Delta_{1v}-\Delta_{6c}$ (10.92 eV), respectively. Overall, quite good agreement between the measured structures and the transitions in the calculated EPM band-structure has been demonstrated by taking the 'scissors operator' correction into account. The structure G may be attributed to the higher lying CP transitions, such as $L_{13v}-L_{13c}$ (12.82 eV) and/or $A_{13v}-A_{13c}$ (12.98 eV) with the calculated photon energy about 12.8 eV as shown in Fig. 2(b). However, the influence of reflectance due to the plasmons of valence electrons [10] should also be considered, since the structure lies at the reflection edge of the VUV spectrum.

In summary, we have presented clear picture for the CPs in wurtzite InN through identifying up to nine electronic transitions in the temperature-dependent optical transmission, photo-luminescence, and VUV reflection spectra in the wide range from 0.5 to 20.0 eV. The fundamental bandgap of intrinsic InN is found to be very close to the recent strongly re-established value of $\sim$1.2 eV after taking into account the Burstein–Moss shift, bandgap renormalization and Urbach band tail effects. The E_1 transition and higher lying CPs are demonstrated by the aid of Adachi's dielectric function model for the VUV reflection spectrum and the EPM approach for the electron band-structure. The temperature dependence of these interband transitions has also been revealed.

Acknowledgements

This work was supported in part by the Natural Science Foundation of China under contract No. 10125416, the Grant-in-Aid for Scientific Research (c) (No. 16560013) from the Ministry of Education, Culture, Sports, Science, and Technology, Japan, and the Venture Business Laboratory of Saga University.

References

[1] T.L. Tansley, C.P. Foley, J. Appl. Phys. 59 (1986) 3241.
[2] V.Y. Davydov, A.A. Klochikhin, R.P. Seisyan, V.V. Emtsev, S.V. Ivanov, F. Bechstedt, J. Furthmuller, H. Harima, A.V. Mudryi, J. Aderhold, O. Semchinova, J. Graul, Phys. Status Solidi B 229 (2002) R1.
[3] J. Wu, W. Walukiewicz, K.M. Yu, J.W. Ager III, E.E. Haller, H. Lu, W.J. Schaff, Y. Saito, Y. Nanishi, Appl. Phys. Lett. 80 (2002) 3967.
[4] T. Matsuoka, H. Okamoto, M. Nakao, H. Harima, E. Kurimoto, Appl. Phys. Lett. 81 (2002) 1246.
[5] T.V. Shubina, S.V. Ivanov, V.N. Jmerik, D.D. Solnyshkov, V.A. Vekshin, P.S. Kop'ev, A. Vasson, J. Leymarie, A. Kavokin, H. Amano, K. Shimono, A. Kasic, B. Monemar, Phys. Rev. Lett. 92 (2004) 117407.
[6] K.S.A. Butcher, J. Cryst. Growth 269 (VII) (2004) Preface for the Proceedings of the First International Indium Nitride Workshop, Fremantle, Australia, Nov. 16–20, 2003.
[7] M. Kuball, J.W. Pomeroy, M. Wintrebert-Fouquet, K.S. Butcher, H. Lu, W.J. Schaff, T.V. Shubina, S.V. Ivanov, A. Vasson, J. Leymarie, Phys. Status Solidi A 202 (2005) 763.
[8] Q.X. Guo, T. Tanaka, M. Nishio, H. Ogawa, X.D. Pu, W.Z. Shen, Appl. Phys. Lett. 86 (2005) 231913.
[9] A. Kasic, E. Valcheva, B. Monemar, H. Lu, W.J. Schaff, Phys. Rev. B 70 (2004) 115217.
[10] Q.X. Guo, H. Ogawa, A. Yoshida, J. Electron Spectrosc. Relat. Phenom. 79 (1996) 9.
[11] F. Bechstedt, J. Furthmüller, J. Cryst. Growth 246 (2002) 315.
[12] C.P. Foley, T.L. Tansley, Phys. Rev. B 33 (1986) 1430.
[13] Y.C. Yeo, T.C. Chong, M.F. Li, J. Appl. Phys. 83 (1998) 1429.
[14] D. Fritsch, H. Schmidt, M. Grundmann, Phys. Rev. B 69 (2004) 165204.
[15] S. Adachi, J. Appl. Phys. 68 (1990) 1192.
[16] Q.X. Guo, T. Yamamura, A. Yoshida, N. Itoh, J. Appl. Phys. 75 (1994) 4927.
[17] Q.X. Guo, O. Kato, M. Fujisawa, A. Yoshida, Solid State Commun. 83 (1992) 721.
[18] W.Z. Shen, L.F. Jiang, H.F. Yang, F.Y. Meng, H. Ogawa, Q.X. Guo, Appl. Phys. Lett. 80 (2002) 2063.
[19] B. Arnaudov, T. Paskova, P.P. Paskov, B. Magnusson, E. Valcheva, B. Monemar, H. Lu, W.J. Schaff, H. Amano, I. Akasaki, Phys. Rev. B 69 (2004) 115216.
[20] F. Chen, A.N. Cartwright, H. Lu, W.J. Schaff, Physica E 20 (2004) 308.
[21] S.P. Fu, Y.F. Chen, Appl. Phys. Lett. 85 (2004) 1523.
[22] M. Higashiwaki, T. Matsui, J. Cryst. Growth 269 (2004) 162.
[23] J. Chen, W.Z. Shen, H. Ogawa, Q.X. Guo, Appl. Phys. Lett. 84 (2004) 4866.